
ANALYZING RESTING-STATE fMRI DATA IN MARIJUANA USERS VIA HIGH-ORDER ATTENTION BRAIN NETWORK

Jun-En Ding¹, Shihao Yang¹, and Fegn Liu^{1,†}

¹School of Systems and Enterprises, Stevens Institute of Technology, Hoboken, USA

[†]Corresponding author

ABSTRACT

The sustained use of marijuana significantly impacts the lives and health of people. In this study, we propose an interpretable novel framework called the HOGAB (High-Order Attention Graph Attention Neural Networks) model to analyze local abnormal brain activity in chronic marijuana users in two datasets. The HOGAB integrates dynamic intrinsic functional networks with LSTM technology to capture temporal patterns in fMRI time series of marijuana users. Moreover, we use the high-order attention module in neighborhood nodes for information fusion and message passing, enhancing community clustering analysis for long-term marijuana users. Furthermore, we improve the overall learning ability of the model by incorporating attention mechanisms, achieving an AUC of 85.1% and an accuracy of 80.7% in multigraph classification. In addition, we compare linear machine learning methods and evaluate the effectiveness of our proposed HODAB model. Specifically, we identified the most relevant subnetworks and cognitive regions that are negatively influenced by persistent marijuana use, revealing that chronic marijuana use adversely affects cognitive control, particularly within the Dorsal Attention and Frontoparietal networks, which are essential for attentional, cognitive, and higher cognitive functions. The results show that our proposed model is capable of accurately predicting craving maps and identifying brain maps associated with long-term cravings, and also pinpointing active areas that are important for analysis.

Keywords Marijuana · fMRI · Graph neural network (GNN) · Multigraph classification · Addiction prediction

1 Introduction

The issue of addictive substances has become a pressing concern in the United States, particularly regarding the use and legalization of marijuana. Especially, heavy marijuana has been found to have an impact on brain cognition and other cognitive processes [1, 2]. In the traditional view, addiction is related to brain abnormalities in the nucleus accumbens, prefrontal cortex, and amygdala, which have been investigated using neuroimaging [3, 4, 5]. These changes might influence addictive behavior by altering reward processing, decision-making, and emotional regulation. However, current research posits that addiction isn't a localized phenomenon but a network-level disruption. The brain operates as a complex network, and disruptions in connectivity between different regions may play a crucial role in addiction. Addiction is a network-wide phenomenon with altered functional connectivity patterns, according to studies in the resting-state functional magnetic resonance imaging (fMRI) [6, 7, 8, 9]. Recent studies have utilized fMRI to investigate brain activity through methods related to brain networks, providing insight into the association between resting and non-resting brain activities [10, 11, 12]. Network analysis has revealed relationships between the characteristics of marijuana use and various aspects of psychopathology. This includes the age of onset of marijuana use, risk factors, environmental influences, and symptoms of infection [11], as well as predictions of marijuana withdrawal and treatment through network analysis [10].

With advancements in artificial intelligence technology and machine learning methods, several approaches have been developed to provide interpretable explanations for the risks associated with marijuana use on brain networks. These explanations encompass factors such as gender differences, personality characteristics and cognitive abilities, employing

techniques like XGBoost and SHAP values to find the importance of additive variable [13]. Recently, Graph Neural Networks (GNNs) have been used for the analysis of brain networks and fMRI data for diagnosing mental illnesses.

The time series signals of fMRI can construct a graph, where each vertex represents a region of interest (ROI) [14, 15, 16, 17]. In recent researches on brain disorders such as Autism Spectrum Disorder (ASD) and Alzheimer’s Disease (AD), there has been a focus on developing Region of Interest- Graph Neural Network (ROI-GNN) models that can capture features from local to global scales for the purpose of classifying these brain disorders [18]. Alternatively, researchers are constructing functional graph structure feature layers to identify significant brain regions and areas of disease-related activity [18].

However, recent research providing a comprehensive explanation and analysis of network-level alterations in the brains of individuals with marijuana addiction has been limited. In this study, we propose an interpretable HOGAB (High-Order Attention Graph Attention Neural Networks) model for analyzing local abnormal brain activity in long-term marijuana users compared to non-users. Our model’s main contributions include: (1) Being the first to utilize graph deep learning methods to explain the brain network and classify the brain signals of long-term marijuana users, (2) capturing the temporal graph features in the complex fMRI sub-sequences of marijuana users, (3) integrating the functionality of high-order nodes for information fusion and message passing into our model, and (4) providing improved community clustering analysis for long-term marijuana users, and (5) conducting craving brain mapping and predicting functional brain subnetworks regions in the group with long-term marijuana use.

Furthermore, we compared linear machine learning methods and evaluated the effectiveness of our proposed HOGAB. By training the model and reconstructing weighted brain networks, we found that the HOGAB proved to be more effective at analyzing differences between long-term marijuana users and non-users as characterized by functional brain connectivity network.

2 Method

2.1 Problem Definition

In this section, we define each fMRI subject as a supervised multigraph classification problem. Specifically, the input subjects set $\{\mathbf{X}^{(i)}\}_{i=1}^N$ time-series data for individual $\mathbf{X}^{(i)} \in \mathbb{R}^{v \times T}$, where v represents the channel of ROIs present in each node, and T as the length of the time series. We segment these nonoverlapping time series as multiple time series for each ROI, obtaining length T' time series divided into $|K|$ segments. Subsequently, we construct the brain network $\mathcal{G}(\mathcal{E}, \mathcal{V}, \mathbf{X})$ based on the segmented time series $|K|$, where \mathcal{E} and \mathcal{V} denotes edges and vertex (region) set. Let $\mathbf{A}_j^{(i)} \in \mathbb{R}^{n \times n}$ represent the j th segment in time series in the i th subject, with functional connectivity computed based on the k-nearest neighbor (k-NN) graph between the time series of each ROIs. Each sub-adjacency can be stacked as multi-adjacency set $\{\mathbf{A}^{(i)}\}_{i=1}^N$ as presented sub-brain networks $\{\mathbf{G}^{(i)}\}_{i=1}^N$, and corresponding j th labels \mathbf{Y}_j for multi-brain networks classification. The sub-adjacency matrices represent local subnetworks within the entire brain network, allowing for further analysis of local brain abnormalities.

2.2 Model Architecture

The overall framework of HOGAB as shown in Fig. 1. We design a stable multigraph classification architecture and introduce two sub-models in our HOGAB components: (1) intra-view time series model that captures the interdependency of sub-graphs in each segmented time windows and (2) instance-view sequential graph model using LSTM to learn different instance ROI graph signals. The intra-view module uses a higher-order attention mechanism with a neighborhood mixing model to learn the relationship between ROIs after segmenting dynamic time series in the same subject. Meanwhile, we proposed that the LSTM sub-model can better extract local features from the sub-sequential graphs to improve the ability to distinguish between subjects’ brain networks. The overall framework involves more than just feature extraction from a single model. Crucially, concatenating the latent spaces of the two sub-models can lead to more stable model loss convergence.

2.2.1 Intra-view learning with high-order attention neighbor mixing

The proposed intra-view model is able to capture nonoverlapping time series fluctuations signals within each dynamic graph based on segmented sub-sequences. As time progresses within a single instance, constructed sub-sequences to sub-graphs with different timestamps will generate varying graph structures and states. Instead of using the entire time series, our sub-model can learn for temporal connectivity graph to reduce noise at different time points. To prevent the loss of temporal dependencies after segmentation, we designed our sub-model to capture time series information through high-order attention connectivity with similar Regions of Interest (ROIs). However, in traditional Graph

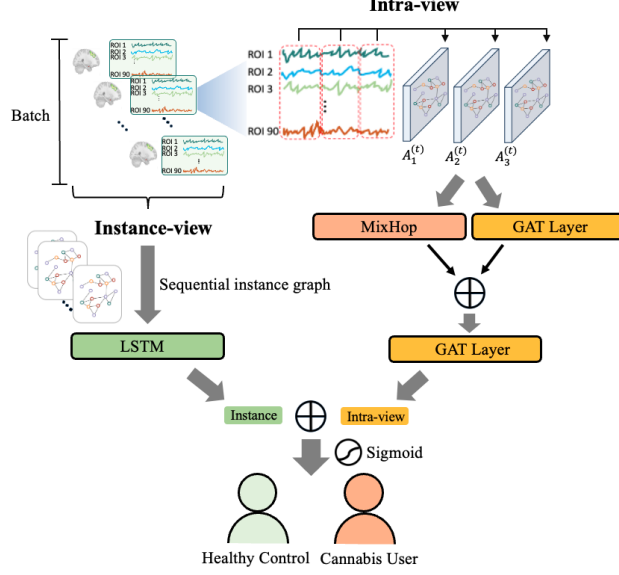


Figure 1: The overall framework of the High-Order attention Brain Network model (HOGAB) utilizes two sub-models to perform fusion learning on fMRI time series. The intra-view model combines mixing hop to conduct high-order attention for message passing. The instance-view uses LSTM to learn the temporal sequence graph and discern differences between instances.

Convolutional Network (GCN) layers, only one-hop connections are utilized for local graph node message passing. The formulated equation of the l -th graph hidden convolutional layer can be defined as follows:

$$\mathbf{M}^{(l+1)} = \sigma(\hat{\mathbf{A}}\mathbf{M}^{(l)}\mathbf{W}^{(l)}), \quad (1)$$

where normalized adjacency matrix $\hat{\mathbf{A}} = \mathbf{D}^{-\frac{1}{2}}(\mathbf{A} + \mathbf{I}_N)\mathbf{D}^{-\frac{1}{2}}$, the $\mathbf{A} + \mathbf{I}_N$ is self-loop connection and $D_{ii} = \sum_i A_{ii}$ is diagonal matrix of \mathbf{A} , \mathbf{W} is a learnable weight matrix in non-linear activation function $\sigma(\cdot)$. By incorporating the neighborhoods of high-order nodes, the MixHop layer [19] used higher-order latent feature learning, which allows learning from their neighbors by incorporating the mixes j -th power of self-adjacency matrix $\hat{\mathbf{A}}^j$, and the two-hop delta operator learns for various neighborhood distances by subtracting different node features. The MixHop graph convolution layer can be defined as

$$\mathbf{M}^{(l+1)} = \left\| \sigma(\hat{\mathbf{A}}^j \mathbf{M}^{(i)} \mathbf{W}_j^{(i)}), \right\|_{j \in P} \quad (2)$$

where P is a set of integers representing the powers of the adjacency matrix, and $\|$ represents the column-wise concatenation of multiple learnable weights. This combination within the graph convolutional layers indirectly facilitates information propagation to two-hop neighbors, resulting in the matrices $\mathbf{M}^{l+1} = \{m_1, m_2, \dots, m_n\}$.

2.2.2 Attention with Mixhop fusion

In the first sub-model of our intra-view framework, we simultaneously used MixHop architecture using high-order message passing and GAT layer [20] for multigraph node features fusion in first architecture as shown in Figure 1. The GAT layer with graph attention mechanisms can aggregate neighborhood node fusion with weighted attention score and enhance ROI functional connectivity. We denote the node embedding $\mathbf{H}^0 = \{\vec{h}_1^0, \vec{h}_2^0, \dots, \vec{h}_n^0\}$ from the first graph attention layer and learn the neighbors \mathcal{N}_i of ROI nodes v_j . We can update the parameterized feature vectors h_i and the learnable weights $\mathbf{W}^0 \in \mathbb{R}^{n \times d}$ using the LeakyReLU function to further calculate the importance attention score as Eq. (3)

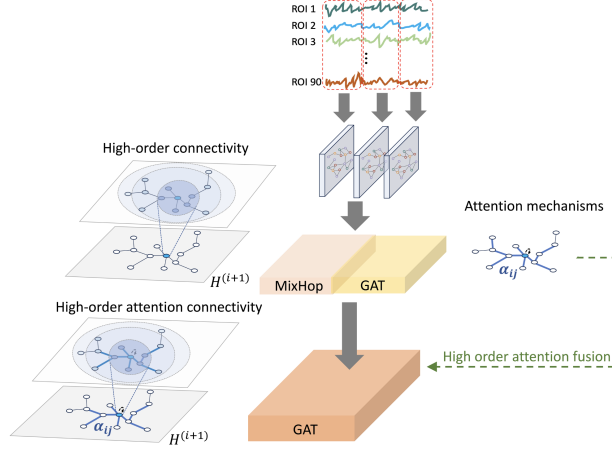


Figure 2: The proposed first sub-model contains MixHop and a graph attention layer, where in the second layer of message passing, concatenating different powers of \hat{A} layers can enhance the depth of attention in the neighborhood node connectivity in pathway.

$$\alpha_{ij} = \frac{\exp\left(\text{LeakyReLU}(\vec{a}_{ij}^T [\mathbf{W}\vec{h}_i \parallel \mathbf{W}\vec{h}_j])\right)}{\sum_{k \in \mathcal{N}_i} \exp\left(\text{LeakyReLU}(\vec{a}_{ij}^T [\mathbf{W}\vec{h}_i \parallel \mathbf{W}\vec{h}_k])\right)}, \quad (3)$$

The attention mechanism generates an importance attention score $\alpha_{ij} \in \mathbb{R}$ for each edge between Regions of Interest (ROIs), enabling the neighboring vertex to better focus on the corresponding node at the edge. Subsequently, we can calculate the features representation \hat{h} of the corresponding nodes through the attention coefficients after a non-linear transformation, as follows:

$$\hat{h} = \sigma \left(\sum_{j \in \mathcal{N}_i} \alpha_{ij} \mathbf{W}\vec{h}_j \right), \quad (4)$$

where $\sigma(\cdot)$ denotes a nonlinear transformation function. In the second layer of the sub-model, we enhance the attention mechanism and the capability for high-order feature fusion within the overall network, as presented in Figure 2. We concatenate embedding vectors m and \hat{h} from the MixHop and GAT layers as the input for the second-layer graph attention layer. However, traditional attention weights for each edge are primarily effective for learning first-order node connectivity, whereas attention MixHop fusion excels at learning second-order neighbor proximity pathways. The concatenated embedding is utilized as the aggregation input for the second-layer \mathbf{GAT}_{l+1} , as follows:

$$\mathbf{H}^a = \mathbf{GAT}_{l+1}(\phi([\mathbf{M} \oplus \hat{\mathbf{H}}])), \quad (5)$$

where \mathbf{M} and $\mathbf{H}^a = [\hat{h}_1^a, \hat{h}_2^a, \dots, \hat{h}_k^a]$ is output features vectors and \oplus is concatenation with according output channel dimensions and $\phi(\cdot)$ is graph global mean pooling $\frac{1}{|\mathcal{V}|} \sum_{i \in \mathcal{V}} \hat{h}_i^{a(l)}$ to average node features across node dimensions.

2.2.3 Sequential Instance Graph Learning

The brain's Regions of Interest (ROIs) exhibit variations in brain networks over time T for each instance. The second sub-model was designed to learn cross-sequential multigraphs between instances and sample a batch of $b \subseteq |K| \times |N|$ sub-graphs from a multigraph set $\{\mathbf{G}_t^{(i)}\}_{i=1}^B$, where B represents the total number of graphs. LSTM (Long Short-Term Memory) networks have been widely used for sequence data, particularly when the goal is to extract local sequential feature information from time series. From time step t , we can formulate the sequence learning representation that includes the input gate \mathbf{I}_t , forget gate \mathbf{F}_t , output gate \mathbf{O}_t , cell gate \mathbf{C}_t and output gate \mathbf{H}^g as shown:

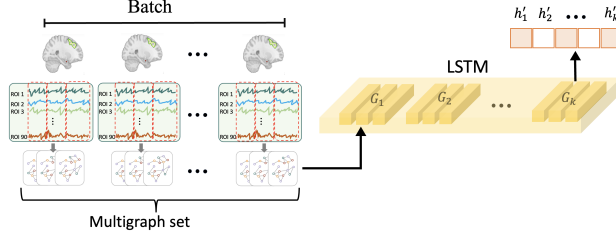


Figure 3: The proposed second sub-model, LSTM, aims to train the graph of each batch instance and learn representations of spatial-temporal dependencies for different subjects.

$$\mathbf{I}_t = \sigma(\mathbf{W}_i \cdot \mathbf{GATconv}(G_t) + \mathbf{W}_i \cdot \mathbf{GATconv}(H_{t-1})) + b_i \quad (6)$$

$$\mathbf{F}_t = \sigma(\mathbf{W}_f \cdot \mathbf{GATconv}(G_t) + \mathbf{W}_f \cdot \mathbf{GATconv}(H_{t-1})) + b_f \quad (7)$$

$$\mathbf{O}_t = \sigma(\mathbf{W}_o \cdot \mathbf{GATconv}(G_t) + \mathbf{W}_o \cdot \mathbf{GATconv}(H_{t-1})) + b_o \quad (8)$$

$$\tilde{\mathbf{C}}_t = \tanh(\mathbf{W} \cdot \mathbf{GATconv}(G_t) + \mathbf{W} \cdot \mathbf{GATconv}(H_{t-1})) \quad (9)$$

$$\mathbf{C}_t = \tanh(\mathbf{I}_t \cdot \tilde{\mathbf{C}}_t + \mathbf{F}_t \cdot \mathbf{C}_{t-1}) \quad (10)$$

$$\mathbf{H} = \mathbf{O}_t \cdot \tanh(\mathbf{C}_t) \quad (11)$$

where \mathbf{W}_i , \mathbf{W}_f , \mathbf{W}_o and \mathbf{W}_c represent learnable weights at different gates and bias vectors b_i , b_f , b_o . By taking output from the LSTM layer, we can get the final instance graph representation:

$$h'_1, h'_2, \dots, h'_k = \mathbf{LSTM}(h_1, h_2, \dots, h_k), \quad (12)$$

where h'_1, h'_2, \dots, h'_k are latent vectors in t -th time step from LSTM modeling. Then we can combine temporal graph features and use graph mean pooling $\phi(\cdot)$ to generate instance representation $\mathbf{H}' = \phi([h'_1 \| h'_2 \| h'_3 \dots \| h'_k])$. To better aggregate two sub-model embedding, we combine two representation \mathbf{H}^a and \mathbf{H}' for final embedding output as shown:

$$\mathbf{H}_i^c = \mathbf{H}^a + \mathbf{H}'. \quad (13)$$

where $\mathbf{H}_i^c \in \mathbb{R}^{B \times C}$ represents the final output and C is the final prediction class, which is a combination of outputs from two sub-models and is utilized to learn information from both perspectives contribution by the sub-models.

2.2.4 Brain network reconstruction and community detection

Functional connectivity is a measure of the brain connections between various regions in marijuana users and non-users. In order to enhance individual brain network connectivity and community clustering, we use the final output embedding \mathbf{H}^c for the network reconstruction by inner-product as:

$$\mathbf{B} = \sigma(\mathbf{H}^c \cdot \mathbf{H}^{c^T}), \quad (14)$$

where $\mathbf{B} \in \mathbb{R}^{n \times n}$ represents the reconstructed matrix for brain Regions of Interest (ROI), we utilize $\sigma(\cdot)$ for a nonlinear transformation to construct a weighted reconstructed matrix. Furthermore, we execute a dot product between the each subjects structure functional connectivity matrices $\mathbf{A}^{(i)}$ and the weighted reconstructed matrix \mathbf{B} to compute the weighted functional connectivity matrix.

$$\mathbf{W}^{FC} = \frac{1}{N} \sum_{i=1}^N \mathbf{B} \cdot \mathbf{A}^{(i)}, \quad (15)$$

After obtaining the weighted functional connectivity \mathbf{W}^{FC} , we further analyze the brain community structure. The concept of community detection in graphs is based on the analysis of edge density. The Girvan-Newman (GN) modularity algorithm is used to determine whether there is a higher degree of similarity between nodes within a community and a lower degree of similarity between nodes outside the community [21, 22]. The GN algorithm follows these steps: (1) calculate the edge betweenness for each edge; (2) remove the edge with the highest edge betweenness; (3) recalculate the edge betweenness for the remaining edges in the network; (4) repeat steps (3) and (4) until any vertex in the network becomes a community. We can compute Modularity M and define community C in graph as:

$$M = \frac{1}{2m} \sum_{ij} (W_{ij}^{FC} - P_{ij}) \delta(C_i, C_j). \quad (16)$$

where m is the total number of edges in the graph, B is the adjacency matrix. We can sum the pairs of pairs of vertex by adjacency matrix with expected edges $P_{ij} = p = 2m/[n(n-1)]$ between i and j in equation (15). The δ -function in terms of vertices i and j belonging to the same community ($C_i = C_j$) clusters in the structure and modularity of the community.

2.2.5 Training and objective function

During the training stage, we can use output embedding in Eq. (5) and Eq. (13) to perform a binary classification task by applying the final non-linear transformation $\sigma(\cdot)$ as:

$$\hat{\mathbf{Y}}_c = \sigma(\mathbf{W}_c^T \mathbf{H}_i^c + b_c), \quad (17)$$

$$\hat{\mathbf{Y}}_{MixGAT} = \sigma(\mathbf{W}_g^T \mathbf{H}_i^g + b_g), \quad (18)$$

where \mathbf{W}_c and \mathbf{W}_g represent trained parameters, and b_c and b_g denote biases. Next, we aim to minimize the overall loss objective function \mathcal{L} derived from the losses of two sub-models. The first is the MixHop attention loss, denoted as \mathcal{L}_{MixGAT} , and the second is the combination fusion model loss from Eq. (13) output embedding, denoted as \mathcal{L}_c . The combined loss can be expressed as:

$$\mathcal{L} = \mathcal{L}_{MixGAT}(\mathbf{Y}, \hat{\mathbf{Y}}_{MixGAT}) + \mathcal{L}_c(\mathbf{Y}, \hat{\mathbf{Y}}_c). \quad (19)$$

where \mathbf{Y} represents the ground truth label, while $\hat{\mathbf{Y}}_{MixGAT}$ and $\hat{\mathbf{Y}}_c$ represent the class predictions for marijuana users and healthy controls, respectively. By combining two \mathcal{L}_{MixGAT} and \mathcal{L}_c , we can better leverage the fusion information in total loss \mathcal{L} not just sub-model loss.

3 Experiments

3.1 Dataset

- **Marijuana-323** In this study, we continued previous author's Kaustubh R. et al [23]. research collected data from two datasets of MRI (Magnetic Resonance Imaging) images consisting of 125 and 198 participants, were recruited from the non-medical marijuana seeking community or from hospitalized patients. Before and after the MRI scan, participants completed the marijuana Craving Questionnaire [24], Marijuana Withdrawal Checklist, and Marijuana Problem Investigation [25]. The data were reprocessed from 3T imaging fMRI data, and an average time series of 90 ROIs was calculated for each subject according to Stanford atlas [26]. In our final training and testing, there were 195 long-term marijuana users and 128 healthy control people.
- **HCP dataset** To validate the effectiveness of HOGAB, we tested the external dataset available from the Human Connectome Project (HCP) S1200, which comprises 1096 Resting-State fMRI (rs-fMRI) scans of young adults. The HCP dataset consists of 598 individuals who have used marijuana, with an average age of 28.76 ± 3.69 , and 493 individuals who have never used marijuana, with an average age of 28.82 ± 3.72 . This data preparation used the first session of each subject and excluded 5 rs-fMRIs that contained less than 1200 frames. The cortical surfaces of each subject were divided into 22 brain regions as ROIs [27] and BOLD (Blood Oxygenation Level Dependent) time series signals were normalized by z-scores [28].

Table 1: Overall multigraph classification performance

Dataset	Model	AUC (%)	Accuracy (%)	Precision (%)	Recall (%)
Marijuana-323	L1 LR	77.7	77.2	78.0	77.7
	L2 LR	75.4	72.8	75.2	75.4
	L1 SVM	79.2	77.9	79.1	79.2
	L2 SVM	77.6	75.6	77.5	77.7
	GCN	77.7	71.5	71.9	71.5
	GAT	81.0	73.8	74.0	73.9
	GraphSAGE	77.3	74.6	75.4	74.6
	BrainGB	83.4	75.0	73.6	69.3
	HOGAB (w/o MixHop)	81.9	76.8	76.8	76.9
	HOGAB (w/o LSTM)	85.1	76.2	76.1	76.2
	HOGAB	85.1	80.7	81.0	80.7
HCP	L1 LR	62.8	62.7	63.3	62.7
	L2 LR	64.9	64.8	65.2	64.8
	L1 SVM	64.6	64.7	64.7	64.7
	L2 SVM	69.6	60.9	64.5	60.9
	GCN	49.9	50.5	25.5	50.5
	GAT	65.6	68.2	68.3	68.2
	GraphSAGE	54.4	53.9	55.7	53.9
	BrainGB	54.4	54.5	52.4	51.9
	HOGAB (w/o MixHop)	70.4	64.8	66.0	64.8
	HOGAB (w/o LSTM)	66.3	67.2	67.3	67.2
	HOGAB	75.5	71.2	71.7	71.7

3.2 Baseline methods

We compared linear methods including Logistic Regression (LR) and Support Vector Machine (SVM), and graph-based methods with some state-of-the-art graph neural networks, including Graph Convolution Network (GCN), GraphSAGE, Graph Attention Network (GAT), GraphSAGE and BrainGNN based on brain network construction pipelines. Linear classifiers were compared using L1 and L2 regularization terms with the original paper.

- **LR with penalty** is a linear classification method that uses Lasso regularization to prevent overfitting. The penalty in L1 or L2 regularization is determined by the sum of the absolute values or the sum of squares of the feature weights. This regularization technique tends to drive the weights of specific features toward zero, leading to the desired effect of feature selection.
- **SVM with penalty** is supervised learning algorithms that will be used for classification and regression analysis tasks. The combination of L1 and L2 penalty terms is referred to as Elastic Net. This is achieved by adding a linear combination of L1 and L2 penalty terms and adjusting the corresponding mixing parameter.
- **Graph Convolution Network (GCN)** is a semi-supervised graph convolutional network model that learns node representations using neighboring information and is commonly used to learn graph structure data.
- **Graph Attention Network (GAT)** is an extension of graph neural networks that introduces an attention mechanism, allowing the model to dynamically adjust the weights of the relationship between different nodes during learning.
- **GraphSAGE** is an inductive graph convolutional network capable of predicting unseen nodes inductively. By employing a sampling strategy, the model learns node embeddings based on the features of neighboring nodes, rather than relying on the entire graph.
- **BrainGB** [29] BrainGB is a platform based on Graph Neural Networks (GNNs) methods, encompassing the prediction of both functional and structural neuroimaging modalities. GNNs are used to model relationships between different brain regions.

3.2.1 Linear classifier

We compare the linear classifier methods including logistic regression as well as support vector machines with L1 and L2 regularization. The table 1 illustrates the model performance between different approaches in Marijuana-323 dataset. In our experiments, we observe that among the linear classification methods—L1 regularized logistic regression, L2

regularized logistic regression, and SVMs regularized with both L1 and L2—the L1 regularized SVM achieved the highest classification accuracy at 79.2%. In HCP dataset, the same linear methods did not achieve better results, only L2 SVM attaining a classification accuracy of 69.6%. The classification results from both datasets indicate that brain fMRI exhibits structured correlations between brain regions, which linear classifiers fail to classify in terms of functional connectivity features.

3.2.2 Graph-level classification

We compared graph-based methods such as GCN, GAT, GraphSAGE and BrainGB as a baseline model and evaluated the HOGAB. In table 1 shows that GAT and BrainGB achieve better AUC scores than linear classifier methods in the Marijuana-323 dataset, but linear models perform better in terms of accuracy, precision, and recall, but only GAT performs robust classification in HCP datasets.

In our ablation experimnts, we verify the contribution of the sub-model of MixHop and LSTM in our overall model framework. First, we removed the high-order fusion of the MixHop model in the HOGAB and observed a significant improvement in AUC, reaching 81.9% and 70.4% compared to the graph-based baseline. This indicates that the overall predictive capability of the model is limited when relying solely on the sequential LSTM. At the same time, we also compared the BrainGB framework, which is specifically designed for the brain network with different message passing or pooling strategies. The experimental results from BrainGB indicate that utilizing only the one-hop neighborhood of local nodes achieves an AUC of 83.4% in the Marijuana-323 dataset but fails to perform adequately in the HCP dataset. Meanwhile, precision and recall are lower than the original GAT model, with values of 73.6% and 69.3%, respectively. Next, we eliminated the influence of LSTM in LOGAB. It was observed that incorporating MixHop into the model significantly enhanced the Area Under the Curve (AUC) for overall brain network learning, achieving 85.1% for Marijuana-323 and 75.5% for the HCP dataset, with accuracies of 80.7% and 71.2%, respectively.

One of the advantages of the HOGAB is its ability to combine two sub-models: one that extracts temporal graph features and another that learns about higher-order attention, eventually fusing the features for more effective messaging. Experimental results demonstrate that it outperforms linear models and other graph-based methods, achieving a significant increase in accuracy at 80.7%, precision at 81.0%, and recall at 80.7% compared to state-of-the-art models.

Next, we evaluated the cross-validation performance of HOGAB by dividing the complete dataset into 5 folds and conducting a 5-fold cross-validation. According to the experimental results shown in Fig. 7, our HOGAB exhibits a notable AUC of $82.4\% \pm 0.029$ in the context of multigraph classification.

3.2.3 Classification of Multi-segment Time Series

In this section, we investigate the impact of segmenting full time series and subsequences into multigraphs with different window sizes T' . In our training strategy, we set four time windows of length $T' \in \{0, 100, 300, 600\}$ for both training and testing. As shown in Fig. 4, it can be seen that AUC, accuracy, F1, and precision are significantly reduced as the number of segmenting fMRI signals increases (segment > 3) in Marijuana-323 data. However, GAT shows a more stable performance when segmenting two or three times compared with GCN. Note that when the number of segmenting is 1, we use the entire signal to construct the graph. In our experiments, the HOGAB exhibits increasingly robust classification performance as the number of segments increases. Specifically, under the optimal condition of segmenting fMRI signals twice, the HOGAB achieves an AUC of 82.7%, accuracy of 79.2%, F1 of 79.26%, and precision of 79.3%.

3.2.4 Ablation study

We conduct ablation studies on sub-model effect to explore the effect of loss function. We designed several optimization experiments to compare the effectiveness of Equation (9) on the overall model learning show in Table 2. Afterwards, we conducted attention mechanism ablation experiments on the effect of multi-heads attentions with each head independently attending to the information from neighboring nodes latent space. After that, we compare the classification effect of different K nearest neighbor parameters on multigraph classification in two datasets.

1. From the experimental results, we compared the performance of solely using \mathcal{L}_c . Our results demonstrate that HOGAB, which integrates two sub-models, achieved an AUC of 78.8% and 66.1% in two datasets, respectively. Furthermore, using only \mathcal{L}_{MixGAT} for the high order attention effect showed no difference from \mathcal{L}_c , and its accuracy, precision, and recall were lower than when using only \mathcal{L}_c in Marijuana-323. It can be observed that \mathcal{L}_c is still capable of preserving the optimization effects of sequence and high-order attention in a single loss function.
2. We believe that combining and optimizing loss functions may be better than using a single loss function. From the results, our experiment using a weight of $\alpha = 0.3$ did not improve the results rather than simply adding the

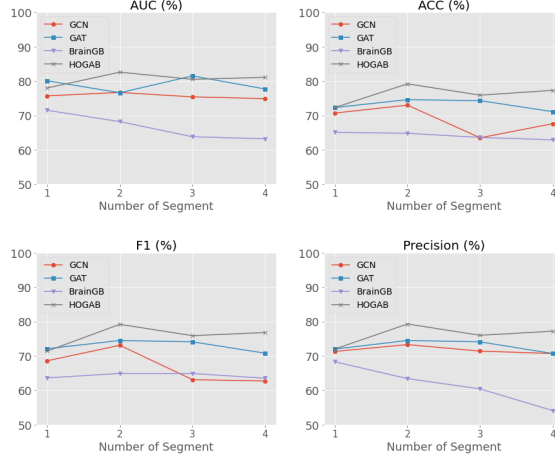


Figure 4: Comparing different models based on their classification performance on Marijuana-323 with different multi-segment time window sizes.

two loss functions $\mathcal{L}_c + \mathcal{L}_{MixGAT}$. This indicates that HOGAB indeed improves optimization by combining the two losses, resulting in a classification AUC of 84.0%, an accuracy of 78.4%, a precision of 78.3%, and a recall of 78.4% in Marijuana-323, and the same as the improvement in performance in HCP.

3. In Figure 8, we increase graph attention multi-heads to capture long-range dependencies and local neighborhoods graph structure. From the results, it can be found that HOGAB in Marijuana-323 and HCP have significant improvement in classification, showing that the increase of attention heads can have a wide of learning node embedding for the high-order connectivity of each sub-graph.
4. We performed groups within the HCP dataset characterized by Marijuana dependence (Mj) and those who have previously used Marijuana, conducting predictions across different age groups. The experimental results indicate that, for the group with Marijuana dependence, our HOGAB predicts the results more accurately in all age groups compared to the group that has only used Marijuana. This indicates that individuals with Marijuana dependence exhibit stronger brain region activity in the BOLD fMRI time series.

Table 2: Classification Performance by Age Group in HCP Dataset

Condition	Age Group	AUC (%)	Accuracy (%)
Mj Dependence	22-25	88.5	92.4
	25-30	89.5	86.4
	30-37	98.8	87.9
Ever Used Mj	22-25	72.1	81.1
	25-30	72.2	63.1
	30-37	70.9	65.9

In order to better analysis regional relationships between ROIs in brain networks, our HOGAB is used to investigate alterations at the level of the functional connectivity networks LM and HC. We reconstruct the Weighted Connectivity (WC) network from the output of the HOGAB to identify a universally interpretable long-term behavioral phenotype of the marijuana brain. We remove the excess density edges of the absolute values and present the weighted connectivity matrix with a density of 2% as shown in Figure 5 (A). Compared to the weighted connectivity of the HC group, certain regions in the LM group exhibit darker colors (burgundy-purple), indicating that long-term marijuana users were more active in the brain region and high connectivity density. To measure connectivity from each region, Degree Centrality (DC) can be define higher connections in nodes and stands out as one of the most direct methods for evaluating centrality. Typically, nodes with higher degrees are located in the center of the network analysis, indicating that they are more importance. Referring to Figure 5 (B), we present the top regions that show the highest average Weighted Connectivity (WC) and DC. It is evident that the areas influencing the LM group encompass Anterior Salience, **Precuneus**, Left Executive Control and Language.

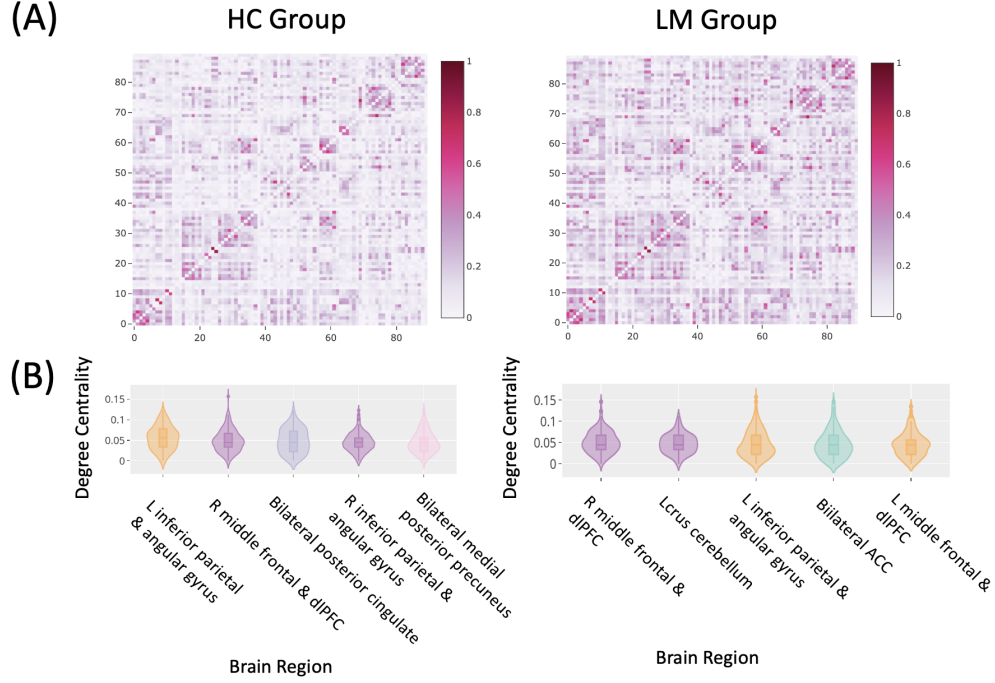


Figure 5: The average of predicted functional Weighted Connectivity (WC) and Degree Centrality (DC) matrix between ROIs in Marijuana-323. Fig. (A) presents the HC and LM group, and (B) presents the corresponding network of the LM group based on the highest WC and DC values in different brain regions.

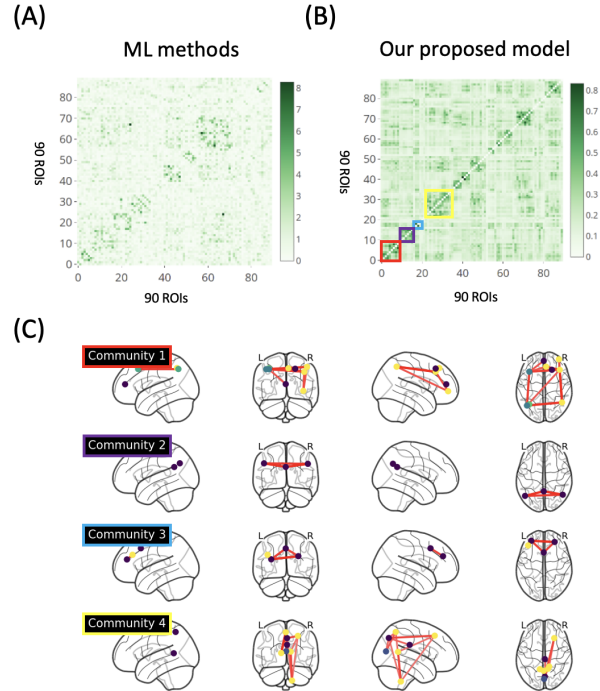


Figure 6: Fig (A) Compare community detection in weighted functional connectivity matrices using machine learning and our HOGAB, where we map the most significant four communities of the LM group to their corresponding brain regions of connectivity network. Based on Fig (B) for the LM group, we drew four communities corresponding to the colored boxes, depicting the connectivity of the most active brain regions in Fig (C).

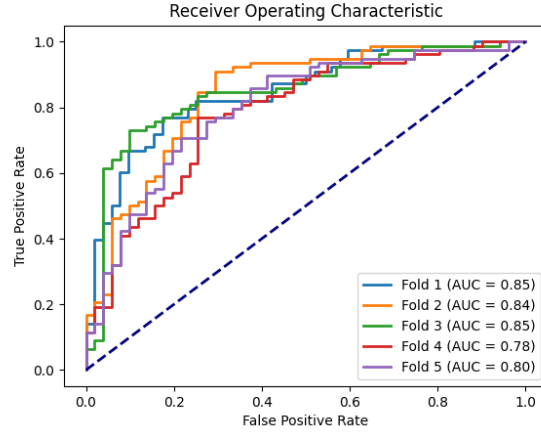


Figure 7: Evaluating AUC performance using five-fold cross-validation on the Marijuana-323 dataset for multigraph classification.

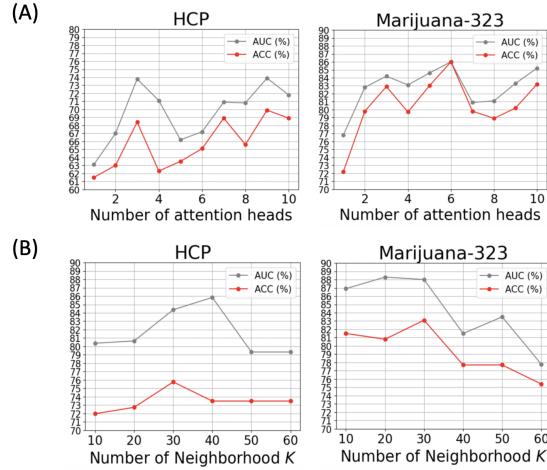


Figure 8: The performance increase from multi-attention heads and K Neighborhood K in the HOGAB.

Table 3: Loss comparison

	Marijuana-323			
	AUC (%)	Accuracy (%)	Precision (%)	Recall (%)
\mathcal{L}_c	78.8	76.9	76.7	76.9
\mathcal{L}_{MixGAT}	78.9	73.9	73.7	73.9
$\alpha \cdot \mathcal{L}_{MixGAT} + (1 - \alpha) \cdot \mathcal{L}_c$	78.9	75.4	75.4	75.4
$\mathcal{L}_c + \mathcal{L}_{MixGAT}$	84.0	78.5	78.3	78.5
	HCP			
	AUC (%)	ACC (%)	Precision (%)	Recall (%)
\mathcal{L}_c	66.1	63.9	63.9	63.9
\mathcal{L}_{MixGAT}	62.4	68.0	68.3	68.0
$\alpha \cdot \mathcal{L}_{MixGAT} + (1 - \alpha) \cdot \mathcal{L}_c$	59.2	62.5	62.5	62.5
$\mathcal{L}_c + \mathcal{L}_{MixGAT}$	70.0	69.1	69.4	69.1

Table 4: Important Brain Connections in Marijuana-323

ROI index	Connection Description
(1, 89)	“L anterior insula” and “R crus cerebellum - visiospatial”.
(4, 89)	“R anterior insula” and “R crus cerebellum - visiospatial”.
(6, 89)	“R crus cerebellum - ant_sal” and “R crus cerebellum - visiospatial”.
(7, 89)	“L superior temporal/auditory” and “R crus cerebellum - visiospatial”.
(10, 89)	“R striatum/thalamus” and “R crus cerebellum - visiospatial”.
(12, 89)	“L inferior frontal gyrus” and “R crus cerebellum - visiospatial”.
(16, 27)	“L lateral angular gyrus” and “L mid-temporal cortex”.
(22, 89)	“L parahippocampal gyrus” and “R crus cerebellum - visiospatial”.
(24, 89)	“L mid occipital cortex” and “R crus cerebellum - visiospatial”.
(26, 89)	“L inferior frontal gyrus” and “R crus cerebellum - visiospatial”.
(28, 89)	“L mid-posterior temporal cortex” and “R crus cerebellum - visiospatial”.
(29, 89)	“L medial angular gyrus” and “R crus cerebellum - visiospatial”.
(30, 89)	“R inferior frontal gyrus” and “R crus cerebellum - visiospatial”.
(31, 89)	“R mid-temporal cortex” and “R crus cerebellum - visiospatial”.
(52, 89)	“bilateral medial posterior precuneus” and “R crus cerebellum - visiospatial”.
(55, 89)	“bilateral calcarine cortex” and “R crus cerebellum - visiospatial”.
(56, 89)	“L LGN” and “R crus cerebellum - visiospatial”.
(63, 64)	“L pre/post-central gyri” and “R pre/post-central gyri”.
(67, 89)	“cerebellar vermis” and “R crus cerebellum - visiospatial”.
(81, 89)	“L precentral/fronto-opercular region” and “R crus cerebellum - visiospatial”.

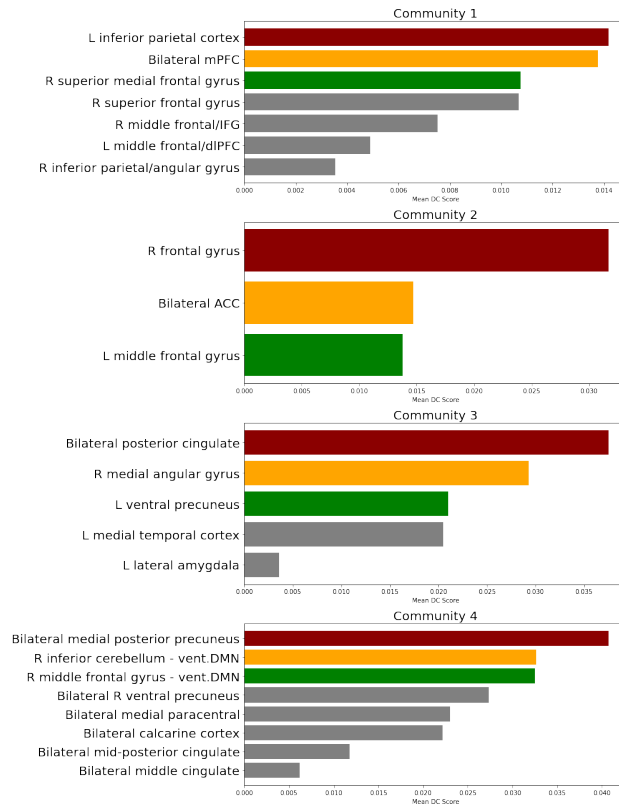


Figure 9: Top 3 LM activate brain regions with Mean DC values across four communities.

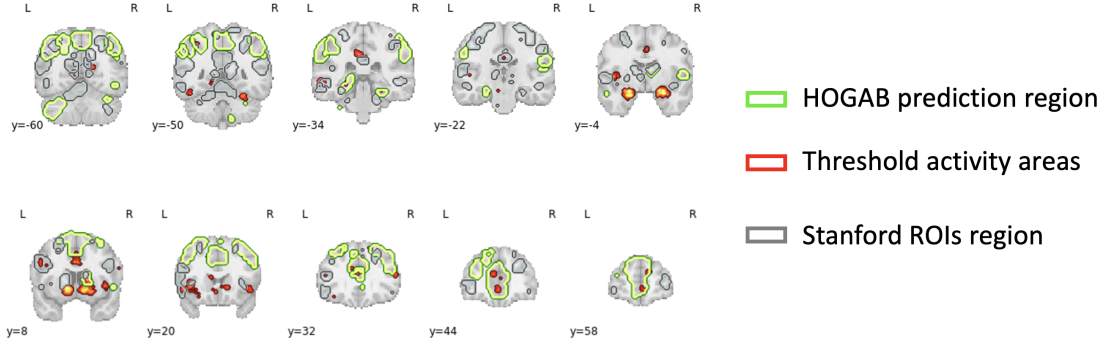


Figure 10: The HOGAB was able to predict craving map (green circle) by utilizing the carving region alongside the gray region of Stanford ROIs, achieving high accuracy in determining overlaps related to chronic marijuana use.

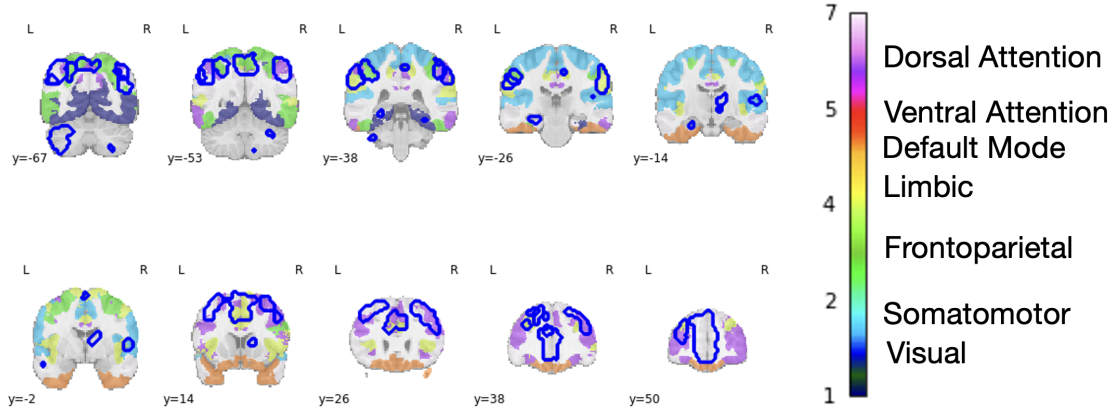


Figure 11: The HOGAB predicts seven subnetwork parcellation of Yeo.

3.2.5 Community clustering

In this study, we explore the community structure within brain networks, emphasizing the significance of clustering for each region based on reconstructed of brain networks from Equation (14). Our analysis includes examining the intricate connections between LM and HC in the brain. This examination is facilitated by integrating the functional connectivity of each instance with the trainable weighted matrix derived from the our HOGAB. Furthermore, by employing the average trainable weighted connectivity matrix, we are able to rank the modularity and degree centrality to identify distinct clusters and community regions, as demonstrated in Fig. 6.

We conducted a comparative analysis between traditional linear machine learning methods and our proposed HOGAB. This comparison, illustrated in Fig. 6, panels A (linear methods) and B (HOGAB), highlights the superiority of the HOGAB in achieving enhanced modularity and clustering effects, particularly in community detection, as substantiated by the results.

As shown in Fig. 6 (C), we circled squares according to the color of each brain cluster region based on their high density degree of centrality. We identified the important brain regions associated with four different communities and sorted the importance scores according to the average DC values. This allowed us to pinpoint critical brain regions linked to four distinct communities. In Table 4, we have followed the indices corresponding to 90 ROIs from Stanford Atlas definition [26] and calculate different Degree Centrality (DC) scores that can be found within the four communities, as shown in Fig. 9. It's reveal the importance rankings of these values, offering insights into the structural and functional connectivity across these brain regions. In our next section on brain analysis, we will analyze and interpret the subnetworks corresponding to the four communities through Yeo seven subnetworks.

3.2.6 Craving maps prediction

Craving maps can aid in deciphering brain network alterations in long-term marijuana users. We aligned the Neurosynth package using the "craving" keyword to identify consistently active brain regions across crave-loaded studies [30]. The uniformity maps displays brain regions consistently activated in studies strongly associated with the term "craving". Based on the cited study's design, an automated meta-analysis of 80 publications identified regions activated by "craving" and Stanford ROIs can be map to uniformity map. Specifically, the uniformity map measures low-activity voxels by removing a threshold of 25% during processing and identifies the activity in each brain region. The identified ROIs on the resulting map can be marked in red as threshold activity areas as shown in Fig. 10. These ROIs represent areas significantly associated with craving, offering a comprehensive view of the brain's response to long-term marijuana use.

Next, we use the HOGAB to predict craving regions based on degree centrality (depicted by the green circle). We then compare these predicted regions to the Neurosynth meta-analytic database using uniformity maps. Finally, we invert the y-axis on the brain volumes within the Stanford ROIs, indicated by the gray circle. The outcomes shown in Fig. 10 demonstrate the precision of our HOGAB in predicting green cravings that are in close alignment with the ROIs across the axes at $y = -60$, $y = 50$, $y = 32$, $y = 44$ and $y = 58$. In our results, we have successfully conducted an analysis of the cognitive-behavioral regions in long-term marijuana users by effectively predicting specific activity regions. The prediction results through our model is able to improve of the prediction consistency and correlation between the network region and the meta-analysis based on specific keywords.

3.2.7 Subnetwork prediction

Researcher Yeo identified functionally coupled regions across the cerebral cortex using the cluster approach based on resting state fMRI data from seven major functional networks in his research [31]. This atlas was created using fcMRI data from 1000 participants to distinguish cortical regions associated with seven parcellations and higher-order cognition. It is proposed that the seven subnetworks be annotated as follows: 1. Visual 2. Somatosensory 3. Dorsal Attention 4. Ventral Attention 5. Limbic 6. Frontoparietal 7. Default. In Fig. 11, we plotted a uniformity map based on Yeo 7 resting-state subnetworks and marked regions predicted by HOGAB (in blue). In the first row, the green regions correspond to overlapping subnetworks at the top of atlas, which are the area of Frontoparietal network associated with cognitive functions such as decision making, problem solving, planning and executive control. In the second row, purple regions represent Dorsal Attention (attention and cognitive control). With Yeo seven subnetworks, we found the HOGAB could identify long-term marijuana users with significant regions in an active transition of cognitive function and attention.

By comparing Yeo seven subnetworks to the four communities in Fig. 9, we can see that the top three regions of each community are well explained by mean DC. Communities 1 and 2 correspond to the Dorsal Attention Network. Communities 4 and 5 correspond to the Frontoparietal Control Network. Finally, Community 3 corresponds to regions that are either part of or closely related to Default Mode Network. According to our study's observations, we can align with previous relevant research that demonstrates that long-term marijuana users exhibit increased subcortical hyperconnectivity, leading to a widespread increase in functional connectivity across the whole brain connectome, particularly in the Dorsal Attention Network and the Default Mode Network [12, 32].

4 Conclusion

In this paper, we propose a mixed model (HOGAB), which incorporates a dynamic graph LSTM capable of learning temporal patterns in fMRI time series and integrates a high-order attention mechanism. Moreover, the HOGAB is more stable than other models for predicting accurate results within multigraph classifications, as well as for clustering networks of long-term marijuana users. By utilizing the HOGAB and Yeo atlas of seven networks, we identified the most relevant subnetworks and cognitive regions that are negatively influenced by persistent marijuana use, revealing that chronic marijuana use adversely affects cognitive control, particularly within the Dorsal Attention and Frontoparietal networks, which are essential for attentional, cognitive control, and higher cognitive functions. Therefore, through the HOGAB, we can more accurately predict craving maps in long-term marijuana users, identify brain maps associated with long-term cravings, and also pinpoint active areas that are important for analysis. In the future, our study not only deepens our comprehension of the effects of long-term marijuana use on the brain, but also underscores the revolutionary potential of AI in functional connectivity in brain networks.

References

- [1] Nadia Solowij and Nicole Pesa. Cognitive abnormalities and cannabis use. *Brazilian Journal of Psychiatry*, 32:531–540, 2010.
- [2] Rebecca D Crean, Natania A Crane, and Barbara J Mason. An evidence based review of acute and long-term effects of cannabis use on executive cognitive functions. *Journal of addiction medicine*, 5(1):1, 2011.
- [3] GAETANO DI CHIARA, G Tanda, VALENTINA BASSAREO, F Pontieri, ELIO Acquas, SANDRO FENU, C Cadoni, and EZIO CARBONI. Drug addiction as a disorder of associative learning: role of nucleus accumbens shell/extended amygdala dopamine. *Annals of the New York Academy of Sciences*, 877(1):461–485, 1999.
- [4] George F Koob and Nora D Volkow. Neurocircuitry of addiction. *Neuropsychopharmacology*, 35(1):217–238, 2010.
- [5] Xavier Noel, Damien Brevers, and Antoine Bechara. A neurocognitive approach to understanding the neurobiology of addiction. *Current opinion in neurobiology*, 23(4):632–638, 2013.
- [6] Nora D Volkow and Marisela Morales. The brain on drugs: from reward to addiction. *Cell*, 162(4):712–725, 2015.
- [7] George F Koob and Nora D Volkow. Neurobiology of addiction: a neurocircuitry analysis. *The Lancet Psychiatry*, 3(8):760–773, 2016.
- [8] Barry J Everitt and Trevor W Robbins. Drug addiction: updating actions to habits to compulsions ten years on. *Annual review of psychology*, 67:23–50, 2016.
- [9] Ning Ma, Ying Liu, Nan Li, Chang-Xin Wang, Hao Zhang, Xiao-Feng Jiang, Hu-Sheng Xu, Xian-Ming Fu, Xiaoping Hu, and Da-Ren Zhang. Addiction related alteration in resting-state brain connectivity. *Neuroimage*, 49(1):738–744, 2010.
- [10] Sarah D Lichenstein, Robert Kohler, Fengdan Ye, Marc N Potenza, Brian Kiluk, and Sarah W Yip. Distinct neural networks predict cocaine versus cannabis treatment outcomes. *Molecular Psychiatry*, pages 1–8, 2023.
- [11] Linda T Betz, Nora Penzel, and Joseph Kambeitz. A network approach to relationships between cannabis use characteristics and psychopathology in the general population. *Scientific reports*, 12(1):7163, 2022.
- [12] JG Ramaekers, NL Mason, SW Toennes, EL Theunissen, and E Amico. Functional brain connectomes reflect acute and chronic cannabis use. *Scientific reports*, 12(1):2449, 2022.
- [13] Gregory R Niklason, Eric Rawls, Sisi Ma, Erich Kummerfeld, Andrea M Maxwell, Leyla R Brucar, Gunner Drossel, and Anna Zilverstand. Explainable machine learning analysis reveals sex and gender differences in the phenotypic and neurobiological markers of cannabis use disorder. *Scientific reports*, 12(1):15624, 2022.
- [14] Xiaoxiao Li, Yuan Zhou, Nicha Dvornek, Muhan Zhang, Siyuan Gao, Juntang Zhuang, Dustin Scheinost, Lawrence H Staib, Pamela Ventola, and James S Duncan. Brainngn: Interpretable brain graph neural network for fmri analysis. *Medical Image Analysis*, 74:102233, 2021.
- [15] Yanqiao Zhu, Hejie Cui, Lifang He, Lichao Sun, and Carl Yang. Joint embedding of structural and functional brain networks with graph neural networks for mental illness diagnosis. In *2022 44th Annual International Conference of the IEEE Engineering in Medicine & Biology Society (EMBC)*, pages 272–276. IEEE, 2022.
- [16] Lingwen Liu, Guangqi Wen, Peng Cao, Tianshun Hong, Jinzhu Yang, Xizhe Zhang, and Osmar R Zaiane. Braintgl: A dynamic graph representation learning model for brain network analysis. *Computers in Biology and Medicine*, 153:106521, 2023.
- [17] Xuan Kan, Antonio Aodong Chen Gu, Hejie Cui, Ying Guo, and Carl Yang. Dynamic brain transformer with multi-level attention for functional brain network analysis. In *2023 IEEE EMBS International Conference on Biomedical and Health Informatics (BHI)*, pages 1–4. IEEE, 2023.
- [18] Hao Zhang, Ran Song, Liping Wang, Lin Zhang, Dawei Wang, Cong Wang, and Wei Zhang. Classification of brain disorders in rs-fmri via local-to-global graph neural networks. *IEEE Transactions on Medical Imaging*, 42(2):444–455, 2022.
- [19] Sami Abu-El-Haija, Bryan Perozzi, Amol Kapoor, Nazanin Alipourfard, Kristina Lerman, Hrayr Harutyunyan, Greg Ver Steeg, and Aram Galstyan. Mixhop: Higher-order graph convolutional architectures via sparsified neighborhood mixing. In *international conference on machine learning*, pages 21–29. PMLR, 2019.
- [20] Petar Velickovic, Guillem Cucurull, Arantxa Casanova, Adriana Romero, Pietro Lio, Yoshua Bengio, et al. Graph attention networks. *stat*, 1050(20):10–48550, 2017.
- [21] Michelle Girvan and Mark EJ Newman. Community structure in social and biological networks. *Proceedings of the national academy of sciences*, 99(12):7821–7826, 2002.

- [22] Santo Fortunato. Community detection in graphs. *Physics reports*, 486(3-5):75–174, 2010.
- [23] Kaustubh R Kulkarni, Matthew Schafer, Laura A Berner, Vincenzo G Fiore, Matt Heflin, Kent Hutchison, Vince Calhoun, Francesca Filbey, Gaurav Pandey, Daniela Schiller, et al. An interpretable and predictive connectivity-based neural signature for chronic cannabis use. *Biological Psychiatry: Cognitive Neuroscience and Neuroimaging*, 8(3):320–330, 2023.
- [24] Stephen J Heishman, Edward G Singleton, and Anthony Liguori. Marijuana craving questionnaire: Development and initial validation of a self-report instrument. *Addiction*, 96(7):1023–1034, 2001.
- [25] Alan J Budney, Pamela L Novy, and John R Hughes. Marijuana withdrawal among adults seeking treatment for marijuana dependence. *Addiction*, 94(9):1311–1322, 1999.
- [26] William R Shirer, Srikanth Ryali, Elena Rykhlevskaia, Vinod Menon, and Michael D Greicius. Decoding subject-driven cognitive states with whole-brain connectivity patterns. *Cerebral cortex*, 22(1):158–165, 2012.
- [27] Matthew F Glasser, Timothy S Coalson, Emma C Robinson, Carl D Hacker, John Harwell, Essa Yacoub, Kamil Ugurbil, Jesper Andersson, Christian F Beckmann, Mark Jenkinson, et al. A multi-modal parcellation of human cerebral cortex. *Nature*, 536(7615):171–178, 2016.
- [28] Soham Gadgil, Qingyu Zhao, Adolf Pfefferbaum, Edith V Sullivan, Ehsan Adeli, and Kilian M Pohl. Spatio-temporal graph convolution for resting-state fmri analysis. In *Medical Image Computing and Computer Assisted Intervention–MICCAI 2020: 23rd International Conference, Lima, Peru, October 4–8, 2020, Proceedings, Part VII* 23, pages 528–538. Springer, 2020.
- [29] Hejie Cui, Wei Dai, Yanqiao Zhu, Xuan Kan, Antonio Aodong Chen Gu, Joshua Lukemire, Liang Zhan, Lifang He, Ying Guo, and Carl Yang. Brainb: A benchmark for brain network analysis with graph neural networks. *IEEE transactions on medical imaging*, 42(2):493–506, 2022.
- [30] Tal Yarkoni, Russell A Poldrack, Thomas E Nichols, David C Van Essen, and Tor D Wager. Large-scale automated synthesis of human functional neuroimaging data. *Nature methods*, 8(8):665–670, 2011.
- [31] BT Thomas Yeo, Fenna M Krienen, Jorge Sepulcre, Mert R Sabuncu, Danial Lashkari, Marisa Hollinshead, Joshua L Roffman, Jordan W Smoller, Lilla Zöllei, Jonathan R Polimeni, et al. The organization of the human cerebral cortex estimated by intrinsic functional connectivity. *Journal of neurophysiology*, 2011.
- [32] Arezoo Taebi, Benjamin Becker, Benjamin Klugah-Brown, Erik Roecher, Bharat Biswal, Jana Zweerings, and Klaus Mathiak. Shared network-level functional alterations across substance use disorders: A multi-level kernel density meta-analysis of resting-state functional connectivity studies. *Addiction Biology*, 27(4):e13200, 2022.